PHYSICAL REVIEW B VOLUME 3, NUMBER 4 15 FEBRUARY 1971

Transport of Heat and Approach to Second Sound in Some Isotopically Pure Alkali-Halide Crystals*

S. J. Rogers†
Laboratory of Atomic and Solid State Physics, Cornell University, Ithaca, New York 14850
(Received 9 September 1970)

The propagation of short thermal pulses has been studied in very pure samples of NaF, Li^7F, and NaI in various crystallographic directions. In each of these crystals the flow of heat at high temperatures is by diffusion, and at the lowest temperatures, by the direct flight of phonons from heater to detector. In the ballistic region, the elastic anisotropy gives rise to a channeling of mode energy into certain preferred directions. Over a limited intermediate temperature range, the effect of normal-process scattering on the propagated heat pulse has been observed in NaF and Li^7F: In the best NaF crystals the pulse velocity approaches the expected second-sound velocity. The observations can be explained satisfactorily in terms of the hydrodynamics of a weakly interacting phonon gas. Computer solutions generated to fit the observed thermal pulse shapes suggest that in NaF, the mean free path for normal-process scattering can be represented by $l_N = 1.42 \times 10^3 T^{-3.71}$ cm in the temperature range 10–20 °K.

I. INTRODUCTION

At low temperatures, when phonon free paths become comparable with sample dimensions, the study of the propagation of short heat pulses yields valuable information concerning the phonon scattering processes in dielectric crystals. This information can be obtained for low-frequency phonons from ultrasonic attenuation measurements, but the mean phonon frequency in a heat pulse is determined by the thermal energy kT and can be much greater than the available ultrasonic frequencies.[1]

Much of the current interest in heat-pulse experiments centers on the mutual scattering of phonons in the three-phonon normal processes (N processes) which conserve the phonon quasimomentum. The scattering cross section for these processes, which do not contribute directly to the thermal resistance, can only be inferred with difficulty from steady-state thermal-conductivity measurements.[2-5] In transient measurements, however, the N processes can play a more dramatic role. By coupling together the various phonon modes, they make possible the collective oscillation in phonon density which has been called second sound. The inertia necessary to sustain this oscillation is provided by the phonon quasimomentum; the resistive scattering of phonons in which this quasimomentum is destroyed will cause damping of the second-sound disturbance.

The possibility that under certain conditions such a temperature wave might propagate in a good thermal conductor was first considered in detail by Ward and Wilks,[6] following an earlier suggestion by Peshkov.[7] On the basis of a phenomenological model they predicted that the velocity of the second-sound disturbance would be $1/\sqrt{3}$ times the mean phonon velocity. More recently, the pioneering work of Krumhansl and his coworkers[8-10] has stimulated a good deal of theoretical interest and provided a more rigorous justification for the concept of second sound in solids. We shall make only passing reference to the rather extensive theoretical literature which has been well reviewed in the papers of Enz[11] and of Ackermann and Guyer.[12]

By contrast, there is a paucity of successful experimental work[13]: A fully developed second-sound pulse has only been observed in solid[12,14] He^4 and solid He^3.[15] These crystals are unusually anharmonic because of their large zero-point motions; it is of interest to consider whether second sound can also be observed in more normal solids. Work on several alkali halides,[16] synthetic sapphire,[17,18] quartz,[19] and more recently the semimetal bismuth,[20] has yielded inconclusive results.

Krumhansl and Guyer[9] have suggested that for second sound to occur the following inequalities must be satisfied:

$$l_N \ll \lambda \lesssim d, \quad l_R \gg d.$$

l_R and l_N are, respectively, the mean phonon paths between resistive and N scattering processes; d is a typical sample dimension; and λ is the wavelength of the disturbance. The crux of the matter is clearly the relative strength of the resistive and N-process scattering of phonons, and it must be remembered that variations in isotopic mass are known to give rise to strong resistive scattering.[21]

For this reason we have in the present work concentrated upon the isotopically pure alkali halides NaF, NaI, and Li^7F. In a preliminary report[22] it was noted that in good NaF crystals the transverse pulse was somewhat delayed in the region of the thermal-conductivity maximum. Further work[23] has shown that this delay represents the

onset of second sound in the crystal; it is the purpose of this paper to discuss these results in more detail.

As will be seen, the full development of the second-sound pulse in even the best NaF crystals is inhibited by the resistive scattering of phonons. The presence of this resistive scattering makes for difficulty in interpreting the data. In order to be more certain of the analysis, we have studied in some detail the effects of resistive scattering at both high and low temperatures. For a given material, temperatures are judged high or low relative to the position of the thermal-conductivity maximum. In the presentation of the experimental results it proves convenient to adopt a threefold division of the temperature range in which intermediate temperatures are considered separately. We term the three temperature regimes ballistic, intermediate, and diffusive, respectively: The ballistic regime is characterized by the direct flight of phonons from heater to detector at the first-sound velocity; at high temperatures, the transport of heat is by diffusion; under certain circumstances the N processes may give rise to hydrodynamic effects at intermediate temperatures.

II. EXPERIMENTAL ASPECTS

A. Crystal Growth and Preparation

The various crystals used in this investigation were all seed pulled from the melt using the Kyropoulos technique. Crystal growth took place in an inert atmosphere of high-purity argon which had been further purified before entering the furnace. The basic techniques have been described in some detail by Peech *et al.*[24]

We were fortunate to have available Thacher's excellent Li^7F crystals[25] ready grown, and sought in the present work to grow NaF and NaI crystals of a comparable quality using the same basic methods.

In the case of NaF, the crystals were grown from two starting materials: Merck ultrapure powder and Harshaw chippings. A preliminary attempt was made to improve these materials by bubbling HF through the melt, but the best available gas donated more impurities – principally Cl – than it removed. The corrosive nature of the molten NaF made purification by zone refining impracticable. However, we tried to achieve the same result by the repeated regrowing of the crystals[26]; at each stage some of the impurities were left behind with the residue of the melt. The final crystal was regrown from its predecessor without breaking the argon atmosphere in the furnace.

As a preliminary check on purity, the absorption spectrum of each boule was measured in the range 1000–4000 cm^{-1} using a modified Beckman IR7 infrared spectrophotometer. The OH^- ion is known to give rise to an absorption peak near 3600 cm^{-1}.[27] It was particularly important to look for this impurity because of its large-resonance cross section for phonon scattering.[28] The best NaF crystals were free of absorption peaks in the near infrared, apart from a weak line in the intrinsic absorption edge at 1140 cm^{-1}. The strength of this line did not, however, correlate with variations in the thermal quality of the crystals. As might be expected, the visible and ultraviolet absorption spectra proved to be a less sensitive guide to crystal purity. Even the poorer samples, with the obvious exception of those containing F centers, showed no absorption in this region.

Steady-state thermal-conductivity measurements were made by Rollefson on those crystals that passed the preliminary spectroscopic screening. The height of the thermal-conductivity maximum is a measure of the integrated scattering of phonons by impurities. These data proved to be the best guide to crystal purity for our purposes. Following earlier practice, the conductivity samples were cleaved to a square cross section of roughly 5 mm on a side. The NaF crystals were then annealed for one hour at 900 °C. Before they were mounted in the cryostat, the crystals were lightly sand blasted to ensure uniformity of behavior in the boundary scattering region.

The conductivity data plotted in Fig. 1[29] show the success of the crystal-regrowing technique.[30] A marked improvement in crystal quality is evident in the sequence of curves A to C for the Merck material. It should be noted that the lowest of these curves corresponds roughly with Walker's data[31] for the best NaF crystal previously measured. The Harshaw material did not respond nearly so well to the regrowing approach; curve D represents the best regrown Harshaw crystal.

Samples were prepared for the heat-pulse experiments in much the same way as for the conductivity measurements, although in this case a flat-plate geometry was used where possible. The [100] samples were cleaved from the boule, but a string saw was used to prepare the [110] and [111] samples. In either case it was necessary to polish the ends of the crystals which were to carry the evaporated films. Prior to annealing, the samples were etched in HF solution to remove surface contamination.

The preparation of Li^7F and NaI samples followed closely the procedures we have described for NaF. NaI, with its affinity for water, presented particular difficulties. In this case the starting material was Merck ultrapure powder, which was always outgassed at 150 °C for 2 or 3 days under vacuum in the furnace before crystal growing was attempted. The regrowing technique was again utilized with a

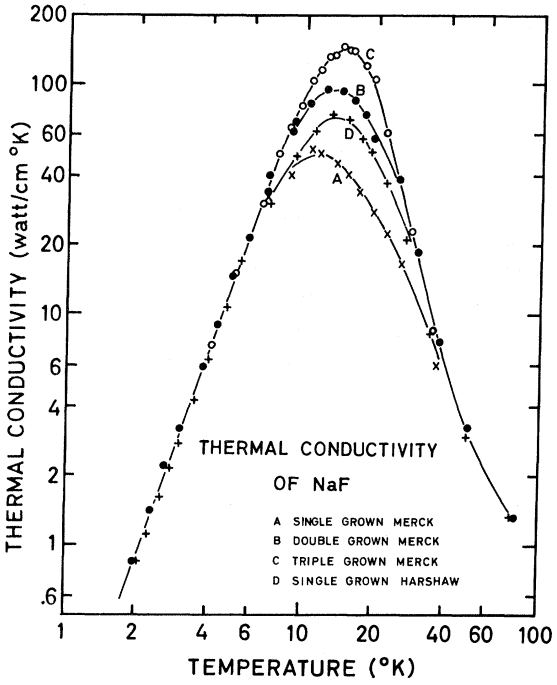

FIG. 1. Thermal conductivity of samples from various boules of NaF: heat flow in [100] direction. Cross sections: A, 4.9×4.7 mm^2; B, 5.2×5.2 mm^2; C, 4.9×5.6 mm^2; D, 4.7×5.0 mm^2.

measure of success which can be judged from the conductivity data of Fig. 2.[29] The NaI heat-pulse samples were polished in a glove box and transferred to and from the evaporator in an evacuated container. Before mounting a crystal in the cryostat, its surfaces, including those which carried the thin metallic films, were coated with J oil to exclude moisture.

As a third check on the purity of the various crystal boules, mass spectrometer analyses were obtained.[32] While there was some ambiguity in the results, the analyses consistently suggested impurity levels which were considerably higher than those specified for the original starting materials. Even the best NaF boule (No. 611-284-2, curve C in Fig. 1) appeared to contain 70 ± 20 ppm of impurity by weight. Chlorine, which contributed nearly half this total, was probably the main source of phonon scattering.

B. Measurement Techniques

The heat-pulse experiments were performed in a simple metal cryostat. The sample was mounted *in vacuo* on a stainless-steel post anchored to the helium bath which could be pumped to 1.8 °K. A heater on the post allowed the sample temperature to be raised above the bath temperature, and a carbon resistance thermometer mounted on the crystal provided a measure of its temperature. The spring-loaded clamp which held the sample was faced with indium to avoid introducing strains into the crystal.

Thin metallic films evaporated onto the ends of the sample served as heater and bolometer; for both purposes a film thickness of about 1000 Å proved to be convenient. Constantan was generally used for the heater, and the resistance of the film was arranged to match the output impedance of the pulse generator. Pure Pb[33] was chosen for the bolometer film which acted as a resistance thermometer. The lead detector was particularly sensitive at its transition temperature of 7.2 °K, but it could also be used at lower temperatures when a magnetic field was applied to destroy partially the superconducting state. Above 7.2 °K, use was made of the ordinary variation of the resistance with temperature. The residual resistance of a film was typically $\frac{1}{40}$ of its room-temperature value, and the fractional sensitivity $d(\ln R)/d(\ln T)$ was greater than unity down to about 13 °K. It will be seen from the data in Fig. 3 that the lead films had a usable sensitivity down to 7.2 °K.

The detector was biased with a constant current so that resistance changes gave rise to a signal voltage across the film. At a given bias power dissipation, the voltage sensitivity for a given

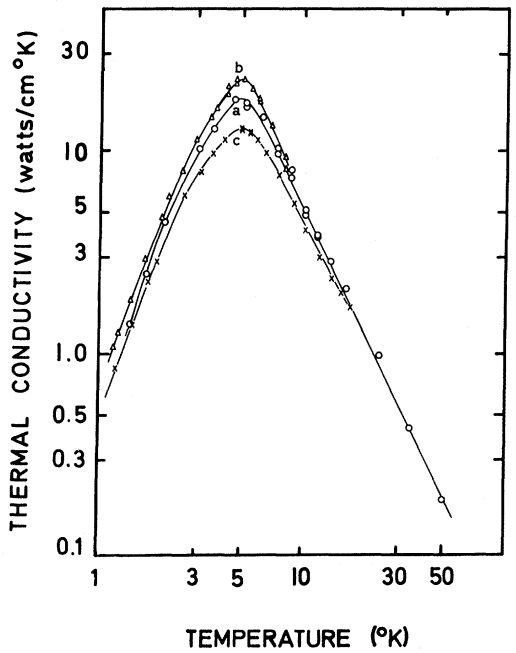

FIG. 2. Thermal conductivity of samples from various boules of NaI: heat flow in [100] direction. a, single grown from Merck powder; b, double grown; c, double grown.

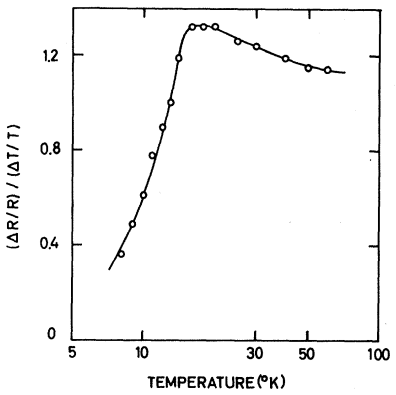

FIG. 3. Fractional sensitivity of typical lead bolometer.

temperature change varies as the square root of the resistance of the detector. In order to increase their resistance, the lead films were evaporated in a zig-zag pattern of some 60 lines to the inch. With this arrangement, the film resistances at room temperature were typically in the range 400–2000 Ω. The detector bias dissipation ranged typically from 0.1 mW at the lowest temperatures up to 0.1 W at high temperatures. However, the associated temperature differences within the crystals rarely exceeded a few millidegrees because of their high thermal conductivities.

A Hewlett Packard type 214A pulse generator supplied the input pulses to the crystal heater; the pulses were typically between 0.1 and 0.5 μsec duration with energies in the range 0.2–200 erg. Assuming a uniform radiation of heat from the heater into the crystal at the mean phonon velocity, the calculated rise in temperature in the region of the heater was generally ≈1%, and always less than 5%, of the mean sample temperature. The signals from the lead detector were usually of a sufficient amplitude to allow their direct display on an oscilloscope after some wide-band preamplification. A Tektronix 1121 amplifier was used in conjunction with a type 547 oscilloscope for this purpose, and the traces were recorded photographically. In a second arrangement, devised to handle weaker signals, a Hewlett Packard 10514A mixer unit was used as the gating element in a box-car circuit in which the gating pulse width was 0.1 μsec; the integrated signal was in this case recorded graphically.

III. THEORETICAL CONSIDERATIONS

In the theoretical analysis we shall adopt an overtly phenomenological viewpoint. Such an approach receives some justification from the work of those authors[11, 34–36] who have considered the phenomenon of second sound in solids in terms of the dynamics of microscopic processes, but the present treatment is perhaps best judged *a posteriori* by its success or otherwise in describing the experimental observations. We shall not concern ourselves with the distinction that has been made between *drifting* and *driftless* second sound[11,37]; we have only observed the approach to second sound, and our measurements would not be sensitive to the predicted 6% velocity difference.

We assume that the thermal excitations in a dielectric crystal can be represented adequately as an isotropic gas of localized weakly interacting phonons, and that the motion of this phonon gas can be described by the usual hydrodynamic equations.[38] In the general case, the equation of motion of a viscous fluid is[39]

$$\rho \frac{\partial \vec{v}}{\partial t} + \rho(\vec{v} \cdot \mathrm{grad})\vec{v} = -\mathrm{grad}P + \eta\nabla^2\vec{v} + (\zeta + \tfrac{1}{3}\eta)\,\mathrm{grad}\,\mathrm{div}\,\vec{v}\,, \tag{1}$$

where $\vec{v}$, P, and ρ are the fluid velocity, pressure, and density, respectively, and η and ζ are the first and second viscosities.

This equation, when applied to the phonon gas, must be rewritten in terms of the heat-flux vector $\vec{F}$, which is the product of the phonon energy density E and the fluid velocity $\vec{v}$. On the left-hand side of the equation, the second term is of second order and can be neglected for small $\vec{v}$, but a further term is needed to represent the resistive scattering of phonons by defects and by the lattice. This *fixed obstacle* term can be written in the relaxation-time approximation as $(\vec{F}/c_1^2\tau_R)$, where c_1 is the average phonon velocity and τ_R is the relaxation time for the resistive scattering of phonons. (Whether or not τ_R equals τ_R^z, the Ziman limit for resistive scattering, will depend upon the strength of the three-phonon N processes.)

Since the fluid momentum $\vec{Q} = \vec{F}/c_1^2$ and the fluid pressure $P = \frac{1}{3}E$, the equation for the conservation of momentum becomes

$$\frac{1}{c_1^2}\frac{\partial \vec{F}}{\partial t} + \frac{\vec{F}}{c_1^2\tau_R} + \frac{C_v}{3}\,\mathrm{grad}T = \left[\eta\nabla^2 + \left(\zeta + \frac{\eta}{3}\right)\nabla(\nabla\cdot)\right]\frac{\vec{F}}{E}\,, \tag{2}$$

where T is the temperature and C_v the specific heat per unit volume.

The corresponding equation for the conservation of energy is

$$C_v\frac{\partial T}{\partial t} = -\,\mathrm{div}\vec{F}\,. \tag{3}$$

The viscous damping term on the right-hand side of Eq. (2) tends to zero in the limit of strong N

processes, and in this limit the two equations combine to give

$$\frac{\partial^2 T}{\partial t^2} + \frac{1}{\tau_R}\frac{\partial T}{\partial t} - \frac{\kappa}{C_v \tau_R}\nabla^2 T = 0\,, \tag{4}$$

where the thermal conductivity $\kappa = \frac{1}{3} C_v c_1^2 \tau_R$. This equation, which has been used by a number of authors,[40,17] yields the characteristic second-sound velocity $c_2 = c_1/\sqrt{3}$ when $\tau_R \to \infty$.

It cannot, however, describe the transition with decreasing phonon-phonon interaction from the second- to the first-sound regime. In our experiments we have been concerned with this transition, and the terms on the right-hand side of Eq. (2) are essential in the analysis.

Ackermann and Guyer[12] have considered these terms in the limit $\tau_N \omega \ll 1$, where τ_N is the relaxation time for N-process scattering and ω is the angular frequency of the thermal disturbance. The first viscosity is then given by $\eta = \frac{1}{3} E \tau_N$. In this limit the second viscosity has the same form and is just twice the first viscosity. With increasing τ_N, η eventually tends to zero and the dominant damping mechanism is provided by the second-viscosity term. By analogy with the hydrodynamic case[41] we shall write the second viscosity as

$$\zeta = \frac{\tau E(1 - c_2^2/c_1^2}{1 - i\omega\tau}\,, \tag{5}$$

where $\tau^{-1} = \tau_N^{-1} + \tau_R^{-1}$ is the combined relaxation rate for all phonon scattering processes. Neglecting η, the wave equation then becomes

$$\frac{\partial^2 T}{\partial t^2} - \tfrac{1}{3} c_1^2 \nabla^2 T + \frac{1}{\tau_R}\frac{\partial T}{\partial t} = \frac{\tau(c_1^2 - c_2^2)}{(1 - i\omega\tau)}\frac{\partial}{\partial t}(\nabla^2 T)\,. \tag{6}$$

Substituting the plane-wave solution $T = T_0 e^{i(kx - \omega t)}$, we obtain the dispersion relation

$$\tfrac{1}{3} k^2 c_1^2 = k^2 c_2^2 = \omega^2 + \frac{i\omega}{\tau_R} + \frac{i\omega k^2 \tau(c_1^2 - c_2^2)}{1 - i\omega\tau}\,. \tag{7}$$

The real and imaginary parts of k determine, respectively, the phase velocity v_p and the attenuation of the wave. The relative phase velocities and the ratio of the imaginary and real parts of k, k_I/k_R are shown in Figs. 4(a) and 4(b). For the case of zero resistive scattering, represented by the solid lines, the phase velocity is c_2 for $\omega\tau \ll 1$ and increases to c_1 at high frequencies. Near $\omega\tau = 1$ the velocity varies rapidly with frequency and, as expected, there is strong attenuation. The opposite limit of $\tau_R = \tau$ is represented by the dotted lines: There is little change in the velocity of high-frequency disturbances, but the wave velocity tends to zero as $\omega \to 0$ and there is strong attenuation at low frequencies.

For simplicity we consider a crystal which is

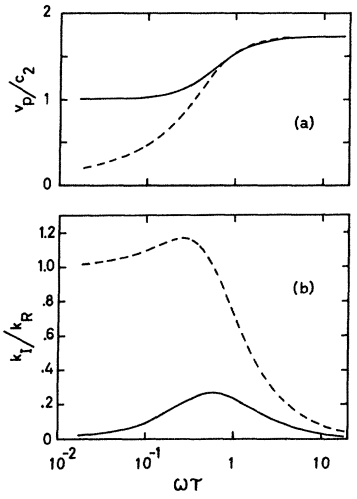

FIG. 4. Graphical presentation of dispersion relationship, Eq. (7): In both figures the solid line is for $\tau_R = \infty$ and the dotted line for $\tau = \tau_R$: (a) Phase velocity of thermal wave of angular frequency ω relative to second-sound velocity; (b) Ratio of imaginary to real parts of propagation constant k.

bounded by the planes $x = 0$ and L and examine the propagation of heat pulses in the x direction. We wish to investigate the solutions of Eq. (6) when a temperature pulse closely resembling a δ function is injected in the plane $x = 0$ at time zero. If necessary, the finite length of the crystal can be allowed for by simultaneously introducing similar temperature pulses in each of the planes $x = \pm 2nL$, where n takes integer values from 1 to ∞. Since the Fourier transform of a δ function is a uniform distribution of equal-amplitude waves of all k vectors from zero to infinity, the initial spatial disturbance can be represented by

$$T(x) = \int_0^\infty \cos(k_R x)\, dk_R\,, \tag{8}$$

where k_R is the real part of the propagation constant. (A normalizing constant is not relevant here and is omitted.) We can replace the integral by the summation

$$T(x) = \lim_{\Delta k_R \to 0} \sum_{n=1}^{\infty} \cos(n\Delta k_R x)\,\Delta k_R\,. \tag{9}$$

The propagation of each of the component waves in this summation will be determined by the dispersion relation (7). At time t the spatial disturbance can therefore be represented by

$$T(x,t) = \lim_{\Delta k_R \to 0} \sum_{n=1}^{\infty} \exp[-(k_I)_n v_n t] \times \cos(n\Delta k_R x - \omega_n t)\,\Delta k_R\,, \tag{10}$$

where v_n, ω_n, and $(k_I)_n$ are, respectively, the phase velocity, frequency, and imaginary propagation

constant of the wave with real wave vector $n\Delta k_R$.

An approximation to the solution in this form can be generated numerically by taking a finite interval Δk_R and setting a finite upper bound to the summation.

IV. NUMERICAL ANALYSIS

The response of the system at a fixed distance L from the heat source is obtained when x is replaced by L in Eq. (10). For the purpose of the analysis, L was usually taken to be unity. The lower bound to the range of k_R vectors needed to approximate the summation is broadly determined by this choice: Wavelengths considerably greater than L are required to represent changes that are slow compared with the time for a phonon to travel this distance. The minimum k_R must, therefore, be much less than $2\pi/L$. In the opposite limit, the upper bound in the summation determines the spatial extent $\pm\delta x$ of the simulated δ function centered on $x=0$ at $t=0$: $\delta x \approx \pi/k_R(\max)$. By varying $k_R(\max)$, the effect on the propagating pulse of changing the duration of the input pulse can be studied.

Within the limits suggested by these considerations, the number of terms used in the summation was dictated by the speed of the available Elliott 4130 computer. The range of k_R values was usually chosen to span some three orders of magnitude, and a summation over 500 equally spaced terms proved generally satisfactory. The input pulse constructed by simply summing over a finite set of k_R vectors was not an ideal δ function. As one would expect, although the pulse could be made arbitrarily narrow, there were always substantial oscillatory disturbances on either side of the central peak. These unwanted oscillations were canceled by superimposing three adjacent wave packets of the simple type.

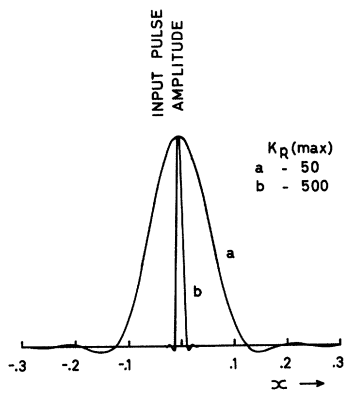

FIG. 5. Simulated input heat-pulse shapes in computer model.

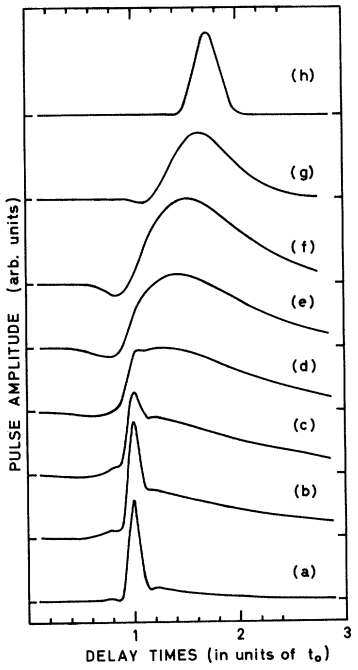

FIG. 6. Detected heat-pulse shapes in computer model at $x=L=1$: $k_R(\max)=50$, $\tau_R=\infty$. τ_N, in units of t_0, is for for various curves: (a) 0.4; (b) 0.2; (c) 0.14; (d) 0.1; (e) 0.07; (f) 0.05; (g) 0.02; (h) 0.0017.

Figure 5 shows the resulting approximation to a δ function for $k_R(\max)=50$ and 500. For the limiting case $\tau_N=\tau_R\to\infty$ of negligible phonon scattering, such pulses are propagated without attenuation or change of shape at the phonon velocity c_1. The effect in the computer model of progressively increasing the strength of the intrinsic N-process interactions is shown in Fig. 6. Here $k_R(\max)=50$, and the unit of time t_0 is the time for a phonon to travel the distance L (= 1). The influence of the N-process scattering is first seen in a rise in level to the right of the ballistic pulse. The direct pulse can be distinguished from this scattered part of the disturbance as long as $l_N \gtrsim \frac{1}{10}L$, where l_N is the mean free path between N processes. For the case $l_N=\frac{1}{10}L$, the beginnings of a distinct second-sound pulse can be seen. The velocity of this pulse falls as the strength of the N-process interaction increases and approaches the second-sound velocity proper for $l_N \lesssim \frac{1}{50}L$.

In the *true* second-sound regime, a decrease in l_N reduces the width of the propagated pulse as required by the calculations of Ackermann and Guyer.[12] We note, however, that where l_N is small, the first viscosity, which is neglected in the present model, will be appreciable. Its effect will be to broaden further the second-sound pulse.

The foregoing pattern of computed results is not much altered by changing the width of the initial

heat pulse. Differences only arise where the pulse (at $L = 1$) has both direct and scattered components. For a given τ_N, very high-frequency components in a pulse will travel at the ballistic velocity [see Fig. 4(a)], and we would therefore expect a reduction in the input pulse width to increase the relative amplitude of the direct component. This proves to be the case, and in the analysis of the results we have chosen our pulse widths to match the experimental observations.

It is implicit in our discussion that variations in L will have no effect on the manner of propagation of the heat pulse. The important parameters in the calculation are L/l_N, $Lk_R(\max)$, etc., and if these are kept constant the results remain the same. However, if l_N is kept constant and L is varied, rapid changes in the pulse profile are to be expected. It will be seen in Fig. 7 that the same l_N can give rise to either ballistic or second-sound propagation depending upon the length of the crystal.

In the computer model, sources at $x = \pm 2L$, $\pm 4L$, etc., can be easily simulated to represent the reflections of the pulse at the planes $x = 0$ and L in a finite crystal. However, these sources can only begin to change the pulse shape at $x = L$ for times greater than $3t_0$ or $3\sqrt{3}\ t_0$ in the ballistic and second-sound regimes, respectively. As we shall see, the reflected signals will generally be masked by the presence of resistive scattering, and we shall ignore them in the subsequent discussion.

When the scattering of phonons by both normal and resistive processes is allowed in the analysis, the range of possibilities becomes too wide for every combination to be considered in detail. We confine our attention here to just two values of the parameter l_N, $\frac{1}{14}L$ and $\frac{1}{500}L$, and examine the effects of resistive scattering in these two cases.

The first represents an intermediate situation in which the velocity of the peak of the disturbance lies between the first- and second-sound velocities;

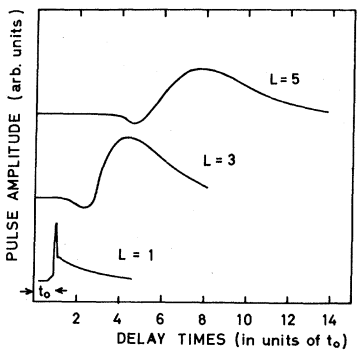

FIG. 7. Computed thermal pulse shapes for different crystal thicknesses: $k_R(\max) = 50$, $\tau_N = 0.2\,t_0$, $\tau_R = \infty$.

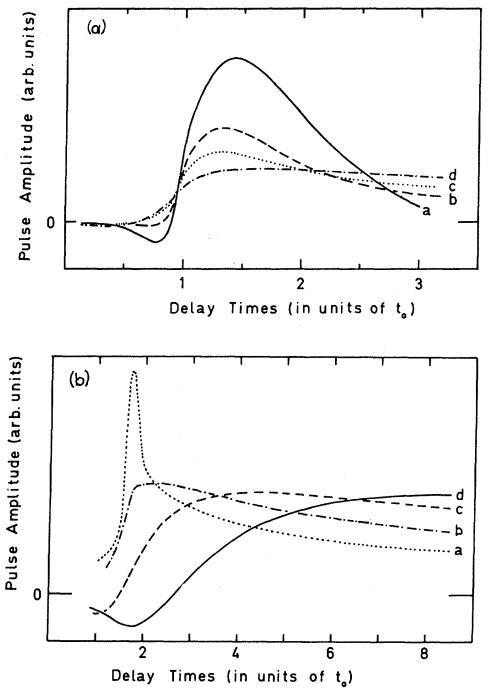

FIG. 8. Effect on computed pulse shapes of resistive scattering. (a) $\tau_N = 0.07\,t_0$. τ_R, in units of t_0, is for various curves: a, ∞; b, 0.95; c, 0.48; d, 0.24. (b) $\tau_N = 0.002t_0$. τ_R, in units of t_0, is for various curves: a, 0.35; b, 0.17; c, 0.085; d, 0.043.

Fig. 8(a) shows computed curves for several values of the resistive mean free path l_R. For small amounts of resistive scattering, a vestige of the direct pulse reappears as a knee in the curve at t_0. This suggests that the resistive processes act preferentially on the scattered rather than the direct component in the pulse, and thus give rise to the unexpected increase in apparent pulse velocity. At the same time, heat scattered out of the main pulse reappears as a long diffuse tail. With increasing resistive scattering the distinct pulse is lost in this diffuse tail.

As a second example we examine the effects of resistive scattering on a fully developed second-sound pulse [Fig. 8(b)]. In this regime, the pattern of computed curves varies little with l_N; here the important parameter is l_R/L. The pulse is easily destroyed by weak resistive interactions and can only be distinguished from the diffuse tail as long as $l_R \gtrsim \frac{1}{4}L$. This requirement is considerably weaker than the condition obtained by Krumhansl and Guyer.[9] On the basis of the present analysis we suggest that a recognizable second-sound pulse will be observed if

$$\tfrac{1}{20}l_N \lesssim L \lesssim 4l_R. \qquad (11)$$

In the limit of strong resistive scattering, $l_R \ll \frac{1}{4}L$, the computed curves approximate closely the known exact solutions of the modified heat equation (4).

In view of its simplicity one would not expect the model considered to account for every detail in the experimentally observed pulse profiles. Different phonon modes and a wide range of phonon frequencies are involved in the real problem, and neither τ_N nor τ_R is independent of mode or frequency. At best we hope to be able to describe the general features of the experimental results.

V. EXPERIMENTAL RESULTS AND DISCUSSION

For convenience of discussion we divide our presentation of results into three sections according to temperature.

A. Ballistic or Boundary-Scattering Region

At temperatures much lower than that of the thermal-conductivity maximum, phonons are scattered only at the boundaries of a single crystal, and in a long thin sample there is the familiar T^3 variation with temperature of the steady-state heat flow. With the usual crystal geometries, the heat-pulse experiments are insensitive to boundary scattering and most of the phonons reach the detector by direct ballistic flight from the heater at their respective mode velocities.

The three oscilloscope traces in Fig. 9 show the detector response when a 0.2-μsec heat pulse is propagated at low temperatures in the [111] direction in NaF. In this direction in the crystal the transverse modes are degenerate and only two pulses are seen. The broadening of the pulses is mainly a geometric effect due to the finite heater and detector areas, and we assume that the initial rise marks the true flight time of each pulse. The first echo of the transverse pulse is seen in the second trace, and when the signal is expanded in

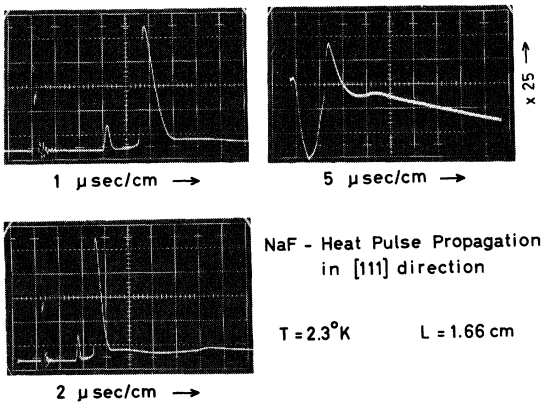

FIG. 9. Heat-pulse propagation in the [111] direction in NaF. Input pulse duration = 0.2 μsec.

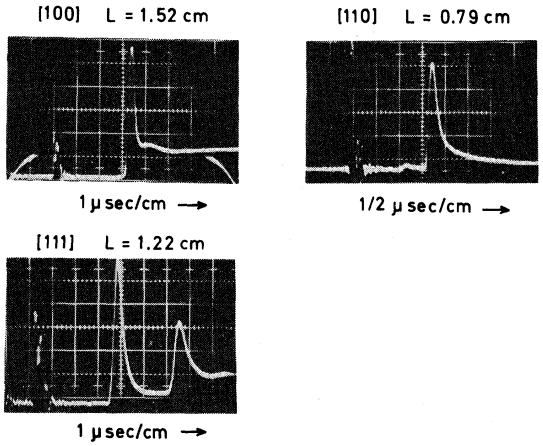

FIG. 10. Heat-pulse propagation at 7.2 °K in the three principal directions in Li^7F. Input pulse durations: [100], 0.3 μsec; [110], 0.1 μsec; [111], 0.2 μsec.

the third trace, a second and perhaps a third echo appear. The diffuse nature of the reflected beam results in a large apparent attenuation. In the best traces no more than four echoes can be resolved.

The velocity of energy propagation[42] in the individual phonon modes can be determined from the oscilloscope traces with a typical accuracy of ±1 or 2%. These velocities, corrected for thermal contraction, are compared in Table I with energy velocities computed from the elastic constants.[43-45] In directions of high symmetry in a cubic crystal, the energy and phase velocities do not differ significantly, but the distinction between these velocities is important for a discussion of the relative amplitudes of the pulses which represent the various phonon modes. It will be seen that for the case of LiF in Fig. 10, the relative mode energies vary considerably with crystallographic direction. Taylor *et al.*[46] have shown that, if it is assumed that phonons are generated at a heat source with a uniform angular distribution of wave vectors, the elastic anisotropy will give rise to a channeling of the energy into certain directions. Broadly speaking, the thermal energy in a given mode will be radiated in those directions in which the velocity and the curvature of the wave surface are at a maximum, but in the three materials studied there are cusps in each of the transverse-wave surfaces which complicate the simple picture.

The density of phonon states in the various modes will also influence the relative amplitudes of the thermal pulses propagated in a given direction. In an isotropic solid, the mode energy for a given temperature rise is inversely proportional to the cube of the mode velocity.

In Table II the observed relative pulse intensities

TABLE I. Measured and calculated thermal energy velocities in NaF, LiF, and NaI.

		Heat-pulse velocities (10^5cm sec^{-1})			Energy velocities (10^5 cm sec^{-1})		
		Longitudinal	Transverse		Longitudinal	Transverse	
NaF	[100]	6.01	3.15		6.22	3.21	
	[110]	5.56	3.89	3.19	5.79	3.92[a]	3.21
	[111]	5.52	3.71		5.65	3.64	3.57[b]
NaI	[100]	2.96	1.40		3.16	1.44	
	[110]	2.71	1.98	1.43	2.85	1.98[a]	1.44
Li^7F	[100]	• • •	4.96		6.86	4.95[a]	
	[110]	(6.97)	4.79	• • •	7.49	4.95[a]	3.94
	[111]	7.59	4.19		7.69	4.28	4.22

[a]Highest velocity, where there is more than one energy velocity associated with a particular mode in a given direction.

[b]Unlike the phase velocities, the energy velocities for the two transverse modes are not exactly degenerate in the [111] direction.

in the principal crystallographic directions for the various materials are compared with intensities calculated for the combined effect of elastic anisotropy and the density-of-states factor. For simplicity, the phonon channeling effect has been estimated by calculating points on the wave surface in the principal crystallographic planes; an angular spread of $\pm 5^\circ$ in the ray vectors was assumed. The calculated enhancement factors are found to be in quite good agreement with the more detailed calculations of Taylor *et al.* when allowance is made for the difference in the assumed angular spread in ray vectors. We note, however, the importance of the density-of-states factor in the analysis. In the [100] direction in NaF, for example, the elastic anisotropy gives rise to an enhancement of the longitudinal pulse by a factor of 2.5, but the transverse pulse is reduced by a similar factor and the dominance of this pulse experimentally arises because of the difference in the mode velocities.

It will be seen that there is generally quite good agreement between the predicted intensities and the experimental observations. Some variation from the calculated intensities is to be expected in the observations because of differences in the heater-bolometer geometries for the various samples; where there is a cusp in the wave surface for a particular mode, as for example in the fast transverse sheet in the [110] direction in LiF, the calculated relative intensities critically depend upon the assumed angular spread of ray vectors. However, for the case of pulse propagation in the [111] direction in LiF, there are no cusps in the velocity surfaces, and it is difficult to account for the difference between the observed and calculated intensities in purely geometric terms.

In an attempt to explain the rather extreme variations in pulse intensity in LiF, experiments were carried out, in which the plane of the heater was not perpendicular to the direction of heat-pulse propagation. The results were essentially unchanged. For example, in an experiment with the heater perpendicular to the [100] direction, the propagated pulses were monitored simultaneously

TABLE II. Comparison of observed and computed relative pulse intensities.

		Observed relative pulse intensities (% total energy)			Calculated relative pulse intensities (% total energy)		
		Longitudinal	Transverse		Longitudinal	Transverse	
NaF	[100]	25	75		33	67	
	[110]	4	73	23	2.5	89	9
	[111]	7	93		6	94	
NaI	[100]	32	68		48	52	
	[110]	10	45	45	6	77	17
Li^7F	[100]	<0.4	100		1	99	
	[110]	3	97	<2	8	84	8
	[111]	63	37		29	71	

in both the [100] and [111] directions; the observed longitudinal pulse was stronger than the transverse pulse in the [111] direction but was zero, as before, in the [100] direction. These observations are consistent with the concept of phonon channeling, but do not rule out the possibility that an acoustic mismatch between the heater and the crystal may influence in some measure the relative pulse intensities.[47] However, Nichrome, Constantan, and Manganin heaters were variously used without any change in the observations. It was clear from the results of several experiments that if there was such an acoustic mismatch, it did not depend critically upon the thickness of the heater film.

There is, nevertheless, some evidence that the generator-crystal interface can play an important role. Hanson[48] experienced considerable difficulty in generating high-frequency longitudinal acoustic waves in the [100] direction in pure LiF with thin-film nickel transducers, but found that weak waves could be generated using oxidized films. Moreover, the longitudinal waves could be readily generated in doped crystals.

It is natural to ask whether the anisotropies in mode intensity which are observed in heat-pulse experiments have any counterpart when there is a steady flow of heat. At high temperatures the thermal conductivity is required to be isotropic by the cubic symmetry of the lattice, but in the boundary-scattering region, anisotropy in the phonon-mode velocities and intensities could give rise to an anisotropy in the transport of heat which would vary with crystal geometry. Brock[49] has calculated that, for a LiF crystal of square cross section with a side-to-length ratio of 1:10, the apparent conductivity in the [111] direction would be some 3% higher than in the [100] direction because of the anisotropy in the mode velocities. The effect of phonon channeling would be to enhance further the preferential heat conduction in the [111] direction.

However, the experimental results in the boundary-scattering region suggest, if anything, a maximum thermal conductivity in the [100] direction: Thacher's[25] data for [100] crystals are consistently some 20% higher than those of Berman and Brock[2] for randomly oriented single crystals. Moreover, the mean free paths for phonons in Thacher's crystals are some 20% greater than the Casimir limit for boundary scattering.[50] In the present work it proved convenient to look for anisotropy in the thermal conductivity of NaF, and measurements were made in the three principal crystallographic directions on samples cut from the same crystal boule. The conductivity in the [110] direction appeared to be somewhat lower than in the [100] and [111] directions, but the differences between samples in the boundary-scattering region were not more than 5% and were barely significant.

It is of some interest to compare phonon mean free paths for the materials studied. Those plotted in Fig. 11(b) have been derived from the thermal-conductivity data of Fig. 11(a) using the simple kinetic-theory expression for the conductivity:

$$\kappa = \tfrac{1}{3} C_v \left(\langle c_1^{-2}\rangle / \langle c_1^{-3}\rangle\right) l_R \,. \tag{12}$$

The velocity averages were approximated by Houston's method.[52] Data for solid He^4 and syn-

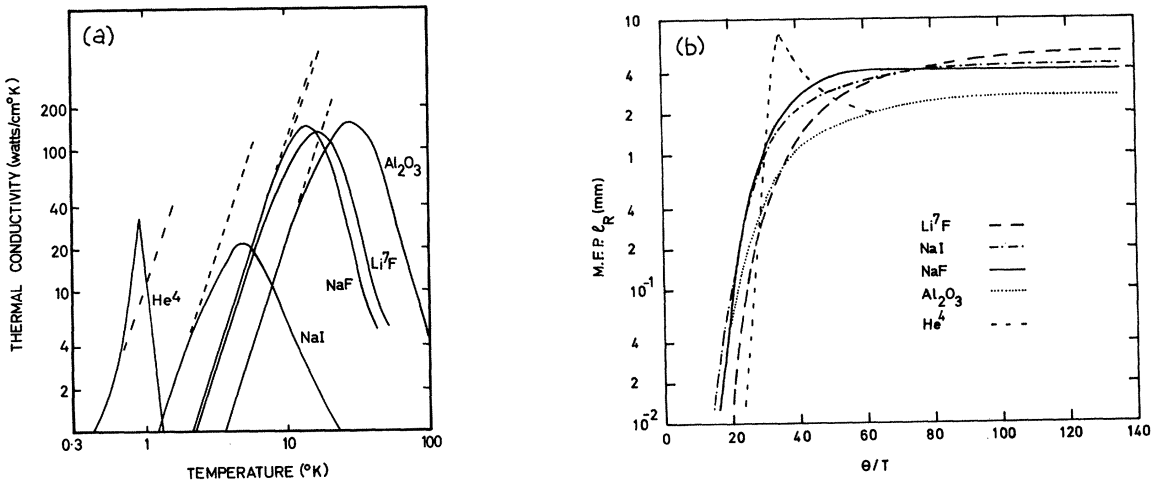

FIG. 11. (a) Comparison of thermal conductivities of some very pure single crystals: NaF and NaI data, curves C in Fig. 1 and b in Fig. 2; Li^7F, Thacher (Ref. 25) (cross section = 4.2×3.8 mm^2); Al_2O_3, Holland (Ref. 51) (cross section = 3.2×3.2 mm^2); He^4, Mezhov-Deglin (Ref. 5) (diam = 2 mm). Dotted lines represent a T^3 variation. (b) Resistive mean free paths derived from conductivity data in (a).

thetic sapphire are included for comparison, but the differences in the sample cross sections should be noted.

It will be seen that in the boundary-scattering region, the phonon mean free path in NaI is roughly 25% more than in NaF for crystals of the same cross-sectional geometry, and that in both materials l_R is substantially less than the Casimir length of ≈ 5.6 mm. The 50% difference in the phonon mean free paths in NaF and LiF is certainly significant. Heat-pulse observations rule out the possibility that the phonon path length in NaF is limited by scattering processes within the body of the crystal, but it is possible that detailed calculations of the effect of phonon channeling on the steady-state flow of heat may resolve the discrepancy.

B. Diffusive Region

In the high-temperature limit, the flow of heat in the crystals will be by thermal diffusion, and the response of the system to a thermal disturbance must satisfy the usual Fourier heat equation

$$\nabla^2 T = \frac{C_v}{\kappa}\frac{\partial T}{\partial t} = \frac{1}{\alpha}\frac{\partial T}{\partial t}, \tag{13}$$

where α is the thermal diffusivity. Two limiting cases arise when we consider a heat-pulse experiment in an infinite slab of solid bounded by the planes $x=0$ and L: the δ-function heat impulse at time $t=0$ can either be distributed uniformly over the plane $x=0$ or be generated at a point in that plane.

The one-dimensional form of Eq. (13) is clearly sufficient to describe the first of these cases, and its solution when a δ-function pulse of heat is injected at $x=0$ and time zero takes the well-known form[53]

$$\Delta T(x,t) \propto 1/\sqrt{t}\; e^{-x^2/4\alpha t}\ . \tag{14}$$

As before, reflections at the faces of the slab can be allowed for by superimposing on this fundamental solution contributions from image sources placed at the planes $x = \pm 2nL$. The solution at $x=L$ which satisfies the boundary conditions is, therefore,

$$\Delta T(x,t) \propto \sum_{n=0}^{\infty} \frac{1}{\sqrt{t}} \exp\left(\frac{-(2n+1)^2 L^2}{4\alpha t}\right)\ . \tag{15}$$

The summation is easily performed numerically and yields a solution which rises asymptotically to its maximum value with increasing time. Following Parker *et al.*[54] and Ackermann and Guyer,[12] we use the tangent to this curve at its steepest point to provide a measure of the thermal diffusivity. This tangent intersects the time axis at time t', where $t' = 0.05L^2/\alpha$. We note, however, that the first term in the summation in Eq. (15) gives a good approximation to the shape of the leading edge of the disturbance and yields for t' the expression

$$t' = 0.048\ L^2/\alpha\ . \tag{16}$$

In the opposite limit of a point source at $x=y=z=0$, the solution of Eq. (13) in an infinite medium takes the form

$$\Delta t \propto (1/t^{3/2})\, e^{-r^2/4\alpha t}\ , \tag{17}$$

where r is the radius vector. It is more difficult in this case to include the effects of reflection in a finite slab of material, but the divergence of the thermal disturbance should make this less necessary. We should expect that in this case, also, the leading term in the solution, Eq. (17), will fairly well approximate the initial shape of the rising edge of the diffuse waveform.[55] For the point $x=L$, $y=z=0$, this term gives for t' the relationship

$$t' = 0.0375L^2/\alpha. \tag{18}$$

The delay times which correspond to t' can be determined with fair accuracy from photographs of the diffuse thermal waveforms. When thermal conductivities are calculated using these times and the known heat capacities, there is better agreement with the steady-state measurements if Eq. (18), the point-source expression for t', is used. This is not very surprising, for in order to reduce boundary effects, the heaters and bolometers were generally confined to the centers of the faces of the crystals.

The general solution of the Fourier heat equation for the case of a finite source of heat in an infinite medium is very complicated, but it reduces to a simple form at points on the x axis for a disk-shaped source which is centered on the origin in the $x=0$ plane. For a source of radius a, the solution for the point $x=L$ can be written[56]

$$\Delta T \propto \frac{1}{t^{1/2}}\left[\exp\left(-\frac{L^2}{4\alpha t}\right) - \exp\left(-\frac{(L^2+a^2)}{4\alpha t}\right)\right]. \tag{19}$$

It is of interest to see how t' derived from this expression varies with a: For $a \gtrsim L$, the solution approaches that for an infinite source and $t' \approx 0.048 \times L^2/\alpha$; if $a \lesssim \frac{1}{4}L$, the solution is close to that for a point source and $t' \approx 0.0375L^2/\alpha$.

The second of these inequalities was usually satisfied in the experiments. We have assumed the validity of the point-source solution in calculating conductivities from the data. Thermal conductivities derived from both transient and steady-state measurements on Li^7F are compared in Fig. 12. The samples were all taken from the same crystal boule, but it will be seen that the apparent conductivity values derived from the heat-pulse observations are nearly 50% higher than the steady-state measurements. This overestimate of the conductivity is typical of all the values derived from the heat-pulse measurements in the three materials

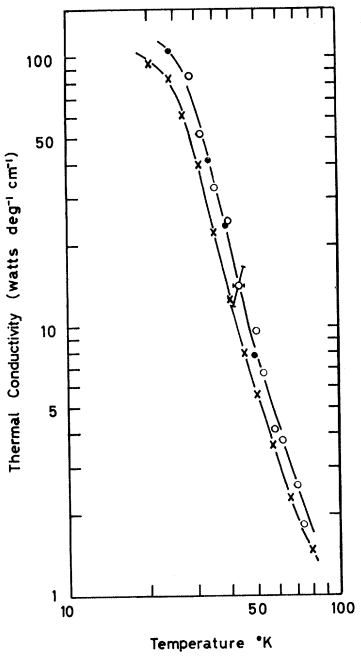

FIG. 12. Thermal-conductivity data for Li^7F: Steady-state data obtained by Thacher, ×; values derived from heat-pulse data using Eq. (18) and known specific heats, ○($L=3.1$ mm), ● ($L=6.4$ mm). Oblique error bar represents effect on calculated conductivity of temperature error of ±2 °K.

studied. Neither the response time of the bolometers nor their finite areas could account for this discrepancy, for both tend to increase rather than decrease the observed values of t'. The high-temperature observations were invariably made as the cryostat warmed up in a situation which only approximated thermal equilibrium. It should be noted that the analysis is particularly sensitive to errors in the temperature measurement: A ±2 °K uncertainty at 43 °K gives rise to the error bar shown in the figure. It seems unlikely, however, that there was an undetected systematic error of +5% in temperature measurements which spanned the range 6–74 °K.

While the heat-pulse data proved a useful and reliable guide to the comparative conductivities of different samples, it would seem that considerable care must be exercised if the absolute values of the conductivities are to be trusted. The sample geometries were far from ideal for these measurements. It may be that more precise results would be obtained with a geometry approaching more closely that of a thin slab with an infinite source.[54] It will be seen in Fig. 13, however, that the point-source solution does fit the observed diffusive waveforms quite well.

C. Intermediate Region

The foregoing analysis breaks down when the diffusive delay t' is of the order of the time t_0 for a phonon to cross the crystal. The temperature at which this occurs will depend upon the length of the crystal since $t' \propto t_0 L/l_R$. At lower temperatures, ballistic propagation will obtain when the mean free path for N-process scattering $l_N \gtrsim L$. Thus, the range of temperatures which we consider in this section will vary with length from sample to sample.

The existence of a third distinguishable temperature range, the hydrodynamic region, depends, as we have seen, upon the strength of the three-phonon N processes relative to resistive scattering. Where the normal interactions are weak we expect that as the temperature is reduced, the diffusive mode of energy transfer will lead directly into the ballistic regime when $t_0 \approx t'$. This proves to be the case in the best NaI crystals we have studied. The main features of the profile of the detected pulses are plotted as functions of the temperature in Fig. 14: The curves, in order of increasing delay, represent, respectively, the leading edge, half-height, and maximum of the ballistic transverse phonon pulse, the maximum of the diffuse pulse, and the peak of the first echo. These observations could imply that the anharmonic coupling between phonons in NaI is relatively weak, but the mean-free-path data of Fig. 11(b) suggest that the strength of the resistive scattering may be the limiting factor.

A rather different pattern emerges when one considers the heat-pulse data for the best NaF crystals. The data shown in Figs. 15(a)–15(c) are for heat-pulse propagation in the [100] direction, but essentially similar results were obtained in the [110] and [111] directions. The two-dimensional representation in Fig. 15(a) is best understood by comparison with Fig. 15(b), where some of the

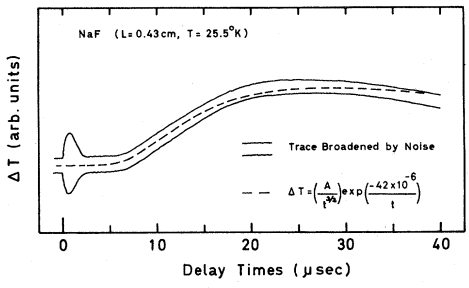

FIG. 13. Comparison of observed diffusive thermal waveform in NaF with Eq. (17). Noise envelope of experimental trace is shown, and electrical breakthrough of the input pulse is seen at time zero.

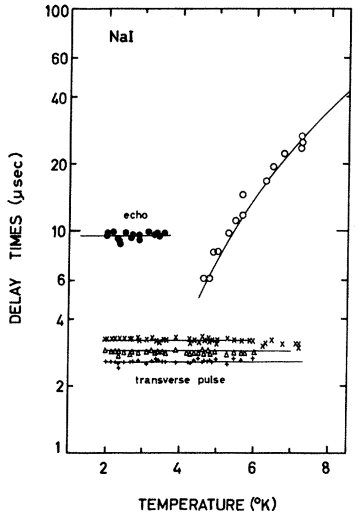

FIG. 14. Heat-pulse propagation in [100] direction in NaI: $L = 3.69$ mm; input pulse width $= 0.4$ μsec. Curves represent the leading edge, forward half-height and peak of transverse pulse, and the peaks of the diffuse pulse and echo.

same data are presented as a three-dimensional graph. The curves in this latter diagram are taken directly from photographs of oscilloscope traces such as those in Fig. 15(c); amplitudes were normalized roughly for convenience by varying the gain of the amplifiers. Two additional features of the main pulse profile are mapped in Fig. 15(a): the solid triangles represent the backward half-height of the pulse; the curve starting at 16 °K represents the leading edge of the main pulse which is distinct from the transverse pulse over a limited temperature range. Delays corresponding to the leading edge and maximum of the longitudinal phonon pulse are also marked on the diagram.

There is a clearly defined range of temperatures about 10–18 °K over which the mode of thermal energy transfer is neither wholly ballistic nor diffusive. In this range, the transverse pulse is increasingly delayed and broadened as the temperature is increased. The separation of the delayed pulse from the remnants of the transverse pulse and the behavior of the longitudinal pulse provide clear evidence that the observed delays are real and not instrumental in origin. Moreover, in the temperature range where this separation is observed, the leading edge of the main pulse is steeper than is the initial rise at lower temperatures. We would expect from the computer analysis that, starting in the ballistic region, the effect of increasing the strength of the three-phonon N processes initially would be to delay and broaden the transmitted thermal pulse. The strength of the N processes in the crystals will certainly increase rapidly with temperature ($\sim T^5$), and the data suggest that we are observing the effects of this increase in three-phonon scattering in the intermediate temperature range.

We assume that the second-sound velocity is given by $c_2 = \frac{1}{2} v_D$, where v_D is the Debye velocity; for the [100] direction in NaF, c_2 defined in this way is very close to $1/\sqrt{3}$ times the transverse velocity. Delays corresponding to c_2 are marked for both direct and reflected pulses in Fig. 15(a). It is interesting to see that these correspond quite well with the maximum observed delays. Unfortunately, it appears that just as the second-sound pulse begins to take shape, it is destroyed by a rapid increase in resistive scattering.

These tentative conclusions receive support when the computer model is used to generate curves to fit the observed wave profiles. In the curve fitting it proved necessary to include resistive scattering. For example, to fit the trace shown in Fig. 16 it was necessary to assume a mean free path of 1.4 mm for resistive scattering. This is twice the mean free path obtained from steady-state measurements at the same temperature, but in view of the preceding discussion concerning diffuse delays, the assumed resistive scattering seems not unreasonable. The N-process scattering needs to be some five times stronger than the resistive scattering to account for the observed trace. In view of the simplicity of the isotropic model assumed, the computer-generated curves fit the observed thermal pulses in the intermediate temperature range quite well. Where l_N is large, a detailed fit depends critically upon the choice of pulse width in the computer program, for, as we have seen, this determines the relative heights of the ballistic and scattered parts of the curve. However, this ambiguity has little influence on the choice of l_N in the region where the main pulse is appreciably delayed.

By using a series of crystals of different lengths, measurements were made in the intermediate temperature region covering a wider range of temperatures than would have been possible with a single crystal. The extent of the intermediate region for these various crystals is shown in Fig. 17. The lower bound plotted on this graph is the temperature at which a delay in the ballistic pulse first becomes apparent. If one assumes that this occurs when the ratio L/l_N has a certain value, one would expect this curve to represent the temperature variation of l_N. In the opposite limit, the upper bound to the region is taken to be the temperature at which there is a sudden rapid increase in the delay of the maxima of the observed pulses. The significance of this temperature is less clear since both normal and resistive scattering processes are involved.

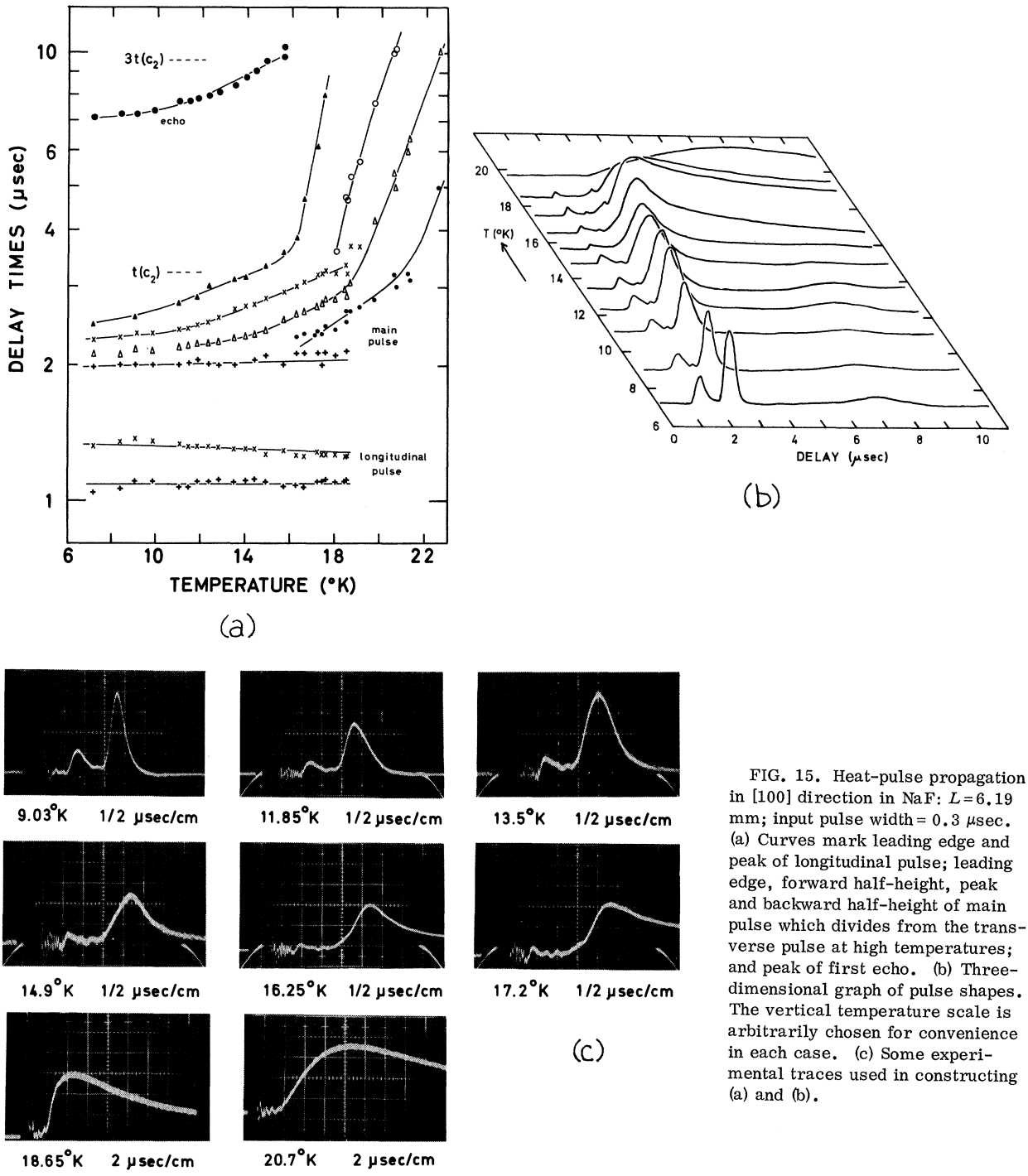

FIG. 15. Heat-pulse propagation in [100] direction in NaF: $L = 6.19$ mm; input pulse width = 0.3 μsec. (a) Curves mark leading edge and peak of longitudinal pulse; leading edge, forward half-height, peak and backward half-height of main pulse which divides from the transverse pulse at high temperatures; and peak of first echo. (b) Three-dimensional graph of pulse shapes. The vertical temperature scale is arbitrarily chosen for convenience in each case. (c) Some experimental traces used in constructing (a) and (b).

The normal-process mean free paths derived from these various data by curve fitting on the computer are plotted as a function of temperature in Fig. 18; for comparison, the resistive mean free paths in Fig. 11(b) are also shown on the graph. The least-squares straight line through the N-process data yields a temperature variation of $T^{-3.71\pm0.26}$ for l_N; $l_N = 1.42 \times 10^3 T^{-3.71}$ cm fits the data. The value obtained is clearly compatible with the theoretical calculations of Herring[57] and of Kwok and Miller[58] and does not differ very significantly from the T^4 variation deduced by Berman and Brock for LiF. The evidence suggests that in the alkali-halide crystals there is a more rapid

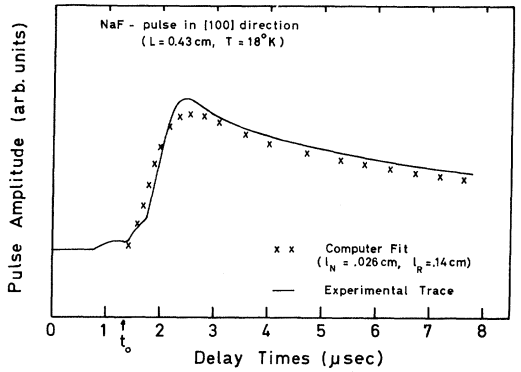

FIG. 16. Comparison of observed and computed pulse shapes in the intermediate temperature range. Peak velocity is very close to the predicted second-sound velocity.

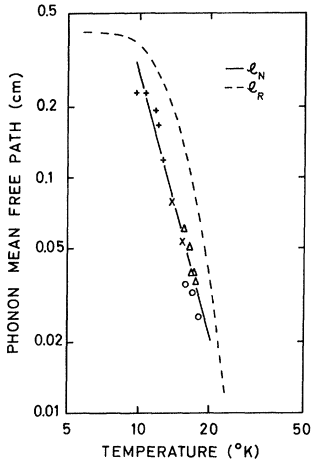

FIG. 18. N-process mean free paths in NaF derived from the observed heat-pulse profiles by curve fitting with computer model. Dotted line representing resistive scattering is from Fig. 11(b).

variation of the N-process scattering than the T^3 variation observed in solid He^4.

It might be argued that the effects we have discussed could be interpreted in terms of some resistive scattering mechanism. If this were the case, it is hard to see why the best NaF crystals should differ so markedly in their behavior from other materials. The scattering strength of most possible crystal defects is either independent of phonon frequency or varies as some positive power of the phonon wave vector q; the scattering of phonons at internal crystallite boundaries, for example, will be frequency independent, but the scattering effect of the strain field surrounding a line dislocation will be proportional to q. At low temperatures, the mean energy $\hbar\omega$ of a thermal phonon will be roughly the same in each of the various phonon modes, and this means that the wave vector q of a typical phonon will be proportional to the mode velocity. Transverse phonons will, on the average, have larger wave vectors than longitudinal phonons and will thus be more subject to those resistive-scattering processes which increase with wave vector.

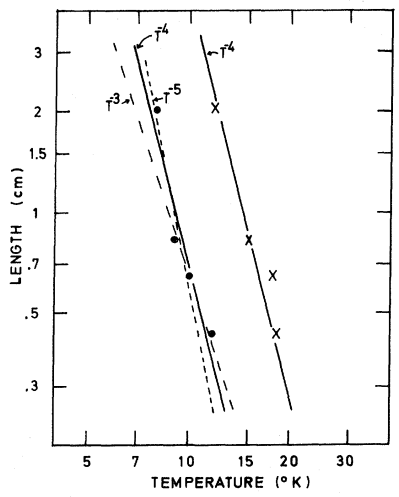

FIG. 17. Variation with crystal length of the extent of the intermediate temperature region for the [100] direction in NaF.

We expect, therefore, that depending on the nature of the process involved, the effect of resistive scattering in a heat-pulse experiment will be either to decrease the amplitude of the transverse pulse relative to the longitudinal pulse or to leave the amplitude ratio unchanged. In the NaF data of Fig. 15, however, it is evident that with increasing temperature the amplitude of the longitudinal pulse *decreases* in comparison with the broadened transverse pulse. The magnitude of this decrease is best seen in Fig. 19, where the ratio of longitudinal to transverse pulse heights is plotted against temperature. This graph underestimates the effect, for no account is taken of the simultaneous broadening of the transverse pulse.

In a series of control experiments the effects on heat-pulse propagation of deliberately introducing resistive scattering centers into the NaF was considered. The first defect chosen for study, the F center, was produced by irradiating the NaF with 140-kV x rays. After 2 h of irradiation with a 10-mA beam, the thermal conductivity[59] at 7 °K was reduced by a factor of 2. There was little change in the relative amplitudes of the longitudinal and transverse pulses over the temperature range in which measurements were made, but

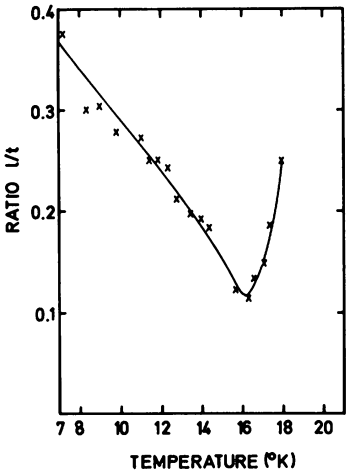

FIG. 19. Ratio of longitudinal to main pulse amplitude for data in Fig. 16. Upturn of the curve at 16 °K may be due to the resistive scattering of phonons.

there was an over-all increase in diffuse scattering. When chlorine was introduced as an impurity into the NaF, the expected preferential scattering of the transverse phonons was observed. In the temperature range where the resistive scattering was appreciable in long crystals, the ratio of the transverse to longitudinal pulse heights was found to decrease rapidly with crystal length. The measurements in Fig. 20 were all made on the same single crystal cleaved progressively; the Cl content of the boule was 600 atomic ppm. It is sometimes said that the Rayleigh scattering of phonons varies as ω^4; the data show directly that it is the wave vector, not the frequency, which determines the scattering cross section.

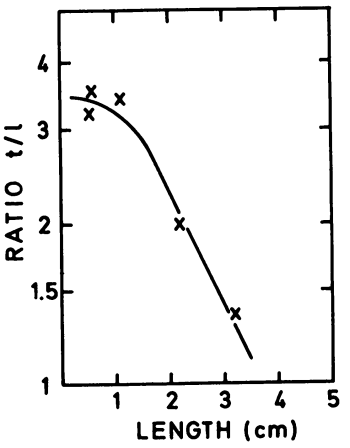

FIG. 20. Ratio of transverse to longitudinal pulse amplitude for heat-pulse transmitted in [100] direction in Cl-doped NaF at 7.2 °K; Cl content was 600 atomic ppm.

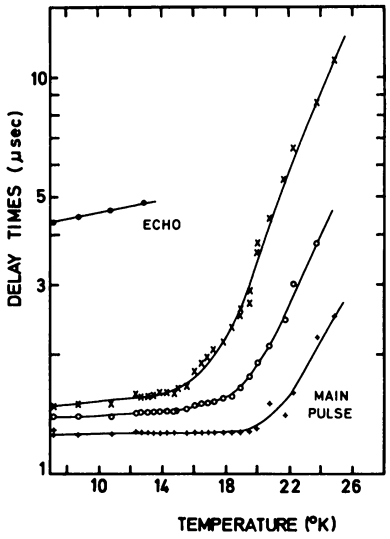

FIG. 21. Heat-pulse propagation in [100] direction in Li^7F: $L = 6.38$ mm; input pulse width = 0.1 μsec. Curves represent the leading edge, forward half-height and peak of the main pulse, and the peak of the echo. There is no longitudinal heat-pulse in this direction in the crystal.

For our present purposes, however, a more important conclusion can be drawn from these experiments, namely, that the two types of resistive scattering considered do not give rise to effects which are in any way similar to those observed in the best NaF crystals. We conclude that the broadening and delay of the main heat pulse in the pure NaF crystals is best accounted for in terms of the nonresistive mutual scattering of phonons.[60]

There is no more than a hint of these effects in the heat-pulse measurements on the best Li^7F samples. Figure 21 is typical of the data for various crystal lengths. It will be seen that with increasing temperature there is only a slight broadening and delay of the transverse phonon pulse. Resistive scattering increases rapidly before the N-process interactions become strong, and it is difficult to extract l_N from the data. We estimate tentatively that at 22 °K, $l_N = 0.025$ cm, but we are not able to ascertain its temperature dependence. This value of l_N is consistent with those obtained from the analysis of the steady-state thermal conductivities. It is, however, three times larger than our estimate of l_N for NaF at the same temperature.

VI. SUMMARY AND CONCLUSIONS

A study has been made of the propagation of short thermal pulses in very pure samples of NaF, Li^7F, and NaI, and steady-state thermal-conductivity measurements have been used as a guide to the interpretation of the results. In each of these materials, the resistive scattering of phonons in-

hibits the full development of a second-sound pulse, but at intermediate temperatures in Li^7F, and particularly NaF, the mutual scattering of phonons by N processes has a marked effect on the pulse profiles. In NaF, the transition from the first- to the second-sound regime is found to occur in the temperature range 10–20 °K and depends upon the length of the crystal.

This transition can be described phenomenologically in terms of the hydrodynamics of a gas of weakly interacting phonons. The second viscosity is mainly responsible for the damping of the thermal waves in such a gas, and also gives rise to a rapid variation in phase velocity when the angular frequency of the disturbance $\omega \approx 1/\tau_N$. The solutions of the hydrodynamic equation which have been generated on the computer give a reasonable representation of the observed pulse shapes when the weak resistive scattering of phonons is taken into account. On the basis of the computer analysis we find that the mean free path for N-process scattering in NaF can be represented by $l_N = 1.42 \times 10^3 T^{-3.71}$ cm in the temperature range 10–20 °K.

A study of the effects of the resistive scattering of phonons both at high temperatures, where the flow of heat is by diffusion, and at low temperatures, where the heat pulses propagate ballistically at the phonon-mode velocities, has convinced us that our interpretation of the phenomena at intermediate temperatures is essentially correct. At low temperatures, the relative pulse intensities are consistent with an analysis in terms of the anisotropic channeling of mode energy into certain crystallographic directions.

ACKNOWLEDGMENTS

The author is much indebted to Professor J. A. Krumhansl and Professor R. O. Pohl for their kind encouragement and advice throughout the tenure of a postdoctoral appointment at Cornell University. The help of R. J. Rollefson, who made the thermal-conductivity measurements, was invaluable, and the assistance of G. E. Schmidt in the crystal growing work is gratefully acknowledged. Thanks are also due to Dr. R. A. Guyer and Dr. J. B. Brown for a number of illuminating discussions.

---

*Research supported by the U. S. Atomic Energy Commission. Additional support was received from the Advanced Research Projects Agency through the Materials Science Center at Cornell University.

†Present address: The Physics Laboratories, The University of Kent at Canterbury, Kent, England. Much of the analysis of the data including the computing was carried out at Canterbury.

[1]Frequencies up to 114 GHz have been used by J. Ilukor and E. H. Jacobsen, who discuss their work in detail in *Physical Acoustics*, edited by W. P. Mason (Academic, New York, 1968), Vol. V.

[2]R. Berman and J. C. F. Brock, Proc. Roy. Soc. (London) A289, 46 (1965).

[3]B. Bertman, H. A. Fairbank, R. A. Guyer, and C. W. White, Phys. Rev. 142, 79 (1966).

[4]R. Berman, C. L. Bounds, and S. J. Rogers, Proc. Roy. Soc. (London) A289, 66 (1965); R. Berman, C. L. Bounds, C. R. Day, and H. H. Sample, Phys. Letters 26A, 185 (1968).

[5]Unique Poiseuille flow data for solid He^4 obtained by L. P. Mezov-Deglin {Zh. Eksperim. i Teor. Fiz. 52, 866 (1967) [Soviet Phys. JETP 25, 568 (1967)]} permits a more direct interpretation: See Ref. 12.

[6]J. C. Ward and J. Wilks, Phil. Mag. 42, 314 (1951).

[7]V. Peshkov, in *Report on Cambridge Low Temperature Conference* (Physical Society, London, 1947), p. 19.

[8]E. W. Prohofsky and J. A. Krumhansl, Phys. Rev. 133, A1403 (1964).

[9]R. A. Guyer and J. A. Krumhansl, Phys. Rev. 148, 778 (1966).

[10]R. A. Guyer and J. A. Krumhansl, Phys. Rev. 148, 766 (1966).

[11]C. P. Enz, Ann. Phys. (N. Y.) 46, 114 (1968).

[12]C. C. Ackermann and R. A. Guyer, Ann. Phys. (N. Y) 50, 128 (1968).

[13]For a recent review see R. J. von Gutfeld, in *Physical Acoustics*, edited by W. P. Mason (Academic, New York, 1968), Vol. V.

[14]C. C. Ackermann, B. Bertman, H. A. Fairbank, and R. A. Guyer, Phys. Rev. Letters 16, 789 (1966).

[15]C. C. Ackermann and W. C. Overton, Phys. Rev. Letters 22, 764 (1969).

[16]R. J. von Gutfeld and A. H. Nethercot, Jr., in *Proceedings of the Ninth International Low-Temperature Conference, Columbus, Ohio*, 1964 (Plenum, New York, 1965), p. 1189.

[17]J. B. Brown, D. Y. Chung, and P. W. Matthews, Phys. Letters 21, 241 (1966).

[18]R. J. von Gutfeld and A. H. Nethercot, Jr., Phys. Rev. Letters 12, 641 (1964); 17, 868 (1966).

[19]J. M. Andrews and M. W. P. Strandberg, Proc. IEEE 54, 523 (1968).

[20]C. R. Brown and P. W. Matthews, Can. J. Phys. 48, 1200 (1970).

[21]P. G. Klemens, in *Solid State Physics*, edited by H. Ehrenreich, F. Seitz, and D. Turnbull (Academic, New York, 1958), Vol. VII, p. 1.

[22]S. J. Rogers and R. J. Rollefson, Bull. Am. Phys. Soc. 12, 339 (1967).

[23]T. F. McNelly, S. J. Rogers, D. J. Channin, R. J. Rollefson, W. M. Goubau, G. E. Schmidt, J. A. Krumhansl, and R. O. Pohl, Phys. Rev. Letters 24, 100 (1970).

[24]J. M. Peech, D. A. Bowers, and R. O. Pohl, J. Appl. Phys. 38, 2166 (1967).

[25]A detailed account of the growth of these crystals will be found in P. D. Thacher, Ph.D. dissertation, Cornell University, 1965 (unpublished). Isotopic separation of the 99.99% Li^7F starting material was carried out at the ORNL. See also P. D. Thacher, Phys. Rev. 156, 975 (1967).

[26]M. F. O'Brien and R. H. Plovnick, Mat. Res. Bull. 4, 671 (1969).

[27]E. Freytag, Z. Physik 177, 206 (1964).

[28]See, e.g., C. K. Chau, M. V. Klein, and B. Wedding, Phys. Rev. Letters 17, 521 (1966).
[29]R. J. Rollefson, Ph. D. dissertation, Cornell University, 1970 (unpublished).
[30]Indirect evidence for the purity of the best of these samples is provided by the work on the effects of impurities on color center formation by M. Meistrich, Ph. D. dissertation, Cornell University, 1967 (unpublished).
[31]C. T. Walker, Phys. Rev. 132, 1963 (1963).
[32]We are indebted to R. K. Skogerboe and the Analytical Laboratory of the Cornell University Materials Science Center for these analyses.
[33]High critical temperature of Pb permits a quite wide range of operation in the superconducting region, and the pure material was chosen in order to achieve a reasonable sensitivity above the transition temperature. J. K. Wigmore [Appl. Phys. Letters 13, 73 (1968)] has reported an interesting bolometer based on the avalanche phenomenon in a doped semiconductor for use at low temperatures in strong magnetic fields.
[34]C. P. Enz, Phys. Letters 20, 442 (1966).
[35]A. Griffin, Phys. Letters 17, 208 (1965).
[36]P. C. Kwok and P. C. Martin, Phys. Rev. 142, 495 (1966).
[37]R. J. Hardy, Phys. Rev. B 2, 1193 (1970).
[38]For a calculation starting from the Boltzmann transport equation see P. Erdos and S. B. Haley, Phys. Rev. 184, 951 (1969).
[39]See, e.g., L. D. Landau and E. M. Lifshitz, *Fluid Mechanics* (Pergamon, Oxford, England, 1959), p. 49.
[40]M. Chester, Phys. Rev. 131, 2013 (1963).
[41]See Ref. 39, p. 307.
[42]The relationship between the phase and energy velocity of acoustic waves in cubic crystals has been discussed in detail by G. F. Miller and M. J. P. Musgrave, Proc. Roy. Soc. (London) A236, 352 (1956).
[43]R. N. Claytor and B. J. Marshall, Phys. Rev. 120, 332 (1960).
[44]C. V. Briscoe and C. F. Squire, Phys. Rev. 106, 1175 (1957).
[45]J. Vallin, K. Marklund, J. O. Sikström, and O. Beckman, Arkiv Fysik 32, 515 (1966).
[46]B. Taylor, H. J. Maris, and C. Elbaum, Phys. Rev. Letters 23, 416 (1969).
[47]Transport of heat across the heater crystal interface has been considered by R. J. von Gutfeld, A. H. Nethercot, Jr., and J. A. Armstrong, Phys. Rev. 142, 436 (1966).
[48]R. C. Hanson, J. Phys. Chem. Solids 28, 475 (1967).
[49]J. C. F. Brock, Ph. D. dissertation, Oxford University, Oxford, England, 1965 (unpublished).
[50]From geometric considerations H. G. B. Casimir calculated that, for a long crystal of square cross section with side d, the mean free path $l=1.12d$ [Physica 5, 495 (1938)].
[51]M. G. Holland, J. Appl. Phys. 33, 2910 (1962).
[52]D. D. Betts, A. B. Bhatia, and M. Wyman, Phys. Rev. 104, 37 (1956).
[53]For a full discussion of the problem, reference should be made to Appendix E of Ref. 12.
[54]W. J. Parker, R. J. Jenkins, C. P. Butler, and G. L. Abbott, J. Appl. Phys. 32, 1679 (1961).
[55]This term has been used successfully in the analysis of heat-pulse propagation in liquid He II at low temperatures [J. M. Ziman, Phil. Mag. 45, 100 (1954)].
[56]See, e.g., H. S. Carslaw and J. C. Jaeger, *Conduction of Heat in Solids*, 2nd ed. (Oxford U. P., London, 1959), p. 260.
[57]C. Herring, Phys. Rev. 95, 954 (1954).
[58]P. C. Kwok and P. B. Miller, Phys. Rev. 146, 592 (1966).
[59]Changes in conductivity which were determined from the heat-pulse measurements were in reasonable agreement with Walker's data (see Ref. 32) for similarly irradiated NaF.
[60]This conclusion has recently received further support from work on still purer NaF crystals [H. E. Jackson, C. T. Walker, and T. F. McNelly, Phys. Rev. Letters 25, 26 (1970)].

PHYSICAL REVIEW B VOLUME 3, NUMBER 4 15 FEBRUARY 1971

Boundary Conditions in Case of Spatial Resonance Dispersion

T. Skettrup
Physics Laboratory III, Technical University of Denmark, Lyngby, Denmark
and
I. Balslev
Physics Institute, Odense University, Odense, Denmark
(Received 21 September 1970)

A simple model accounting for the influence of a surface on polariton waves is introduced. From this the extra boundary condition needed in case of a dispersive resonance is derived. The general result is discussed in relation to actual resonances in crystals. The theory of bulk waves and their boundary conditions is extended to include two or more dispersive resonances. The behavior of the measured exciton lines in ZnO agrees well with the computed spectra.

I. INTRODUCTION

Spatial resonance dispersion[1,2] may be important whenever crystalline excitations that couple to light are able to move. One of the characteristic features of this phenomenon is that two eigenmodes

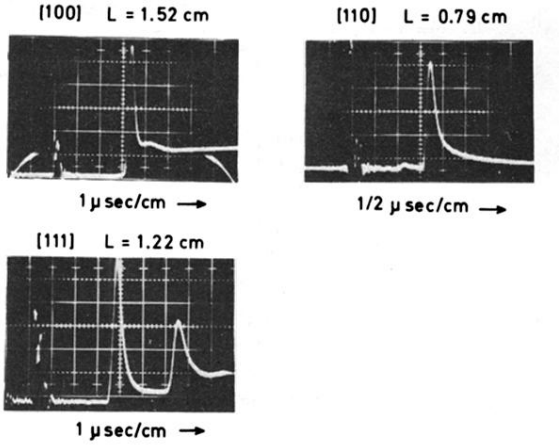

FIG. 10. Heat-pulse propagation at 7.2 °K in the three principal directions in Li^7F. Input pulse durations: [100], 0.3 μsec; [110], 0.1 μsec; [111], 0.2 μsec.

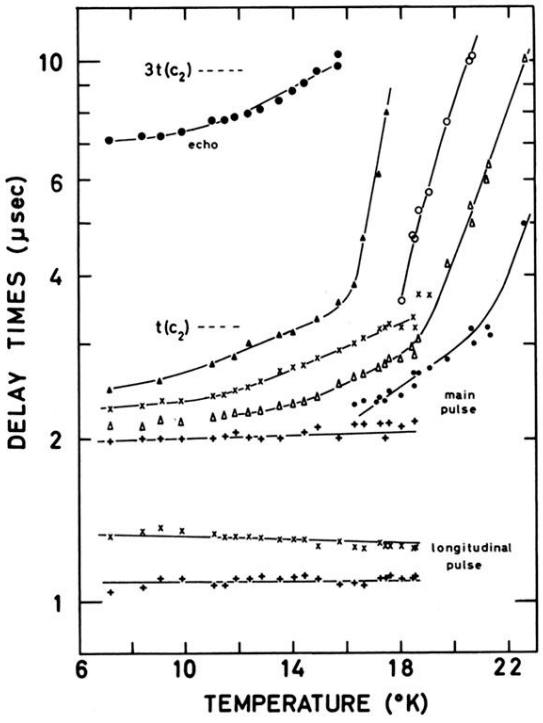

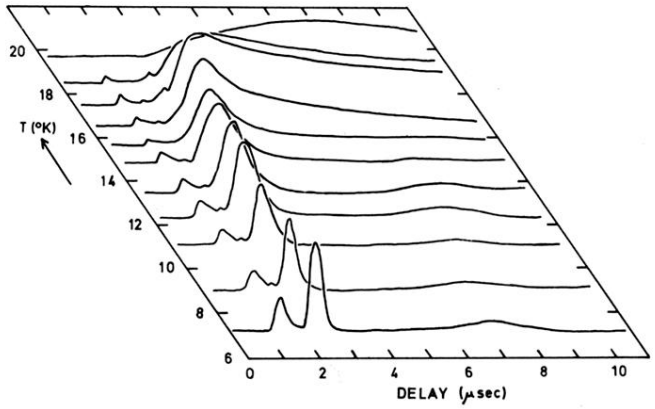

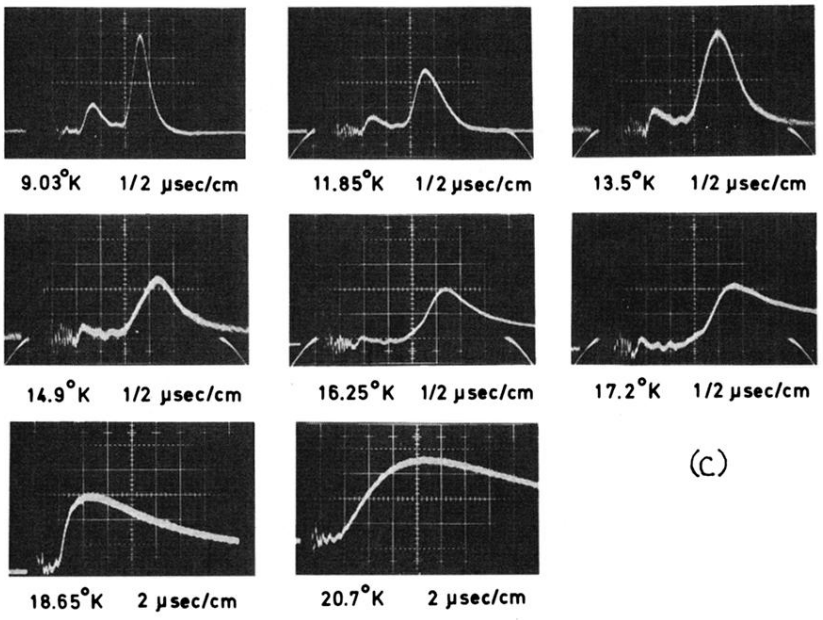

FIG. 15. Heat-pulse propagation in [100] direction in NaF: $L = 6.19$ mm; input pulse width = 0.3 μsec. (a) Curves mark leading edge and peak of longitudinal pulse; leading edge, forward half-height, peak and backward half-height of main pulse which divides from the transverse pulse at high temperatures; and peak of first echo. (b) Three-dimensional graph of pulse shapes. The vertical temperature scale is arbitrarily chosen for convenience in each case. (c) Some experimental traces used in constructing (a) and (b).

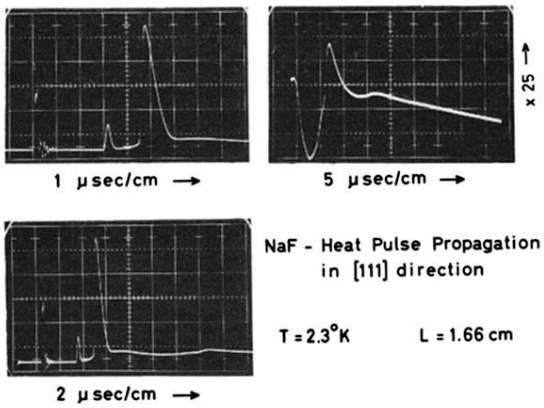

FIG. 9. Heat-pulse propagation in the [111] direction in NaF. Input pulse duration = 0.2 μsec.